MicroRNA-based Regulation of Epithelial-Hybrid-Mesenchymal Fate Determination

Mingyang Lu[1,#], Mohit Kumar Jolly [1,2,#], Herbert Levine[1,2,3*],
Jose' Onuchic [1,3,4,5,*], Eshel Ben-Jacob [1,5,6,*]

[1]Center for Theoretical Biological Physics, [2]Department of Bioengineering, [3]Department of Physics and Astronomy, [4]Department of Chemistry, [5]Department of Biochemistry and Cell Biology, Rice University, Houston, TX 77005-1827, USA
[6]School of Physics and Astronomy and The Sagol School of Neuroscience,
Tel-Aviv University, Tel-Aviv 69978, Israel

Supporting Information

1. The core regulatory network and its coupling with other networks

The core regulatory network for epithelial-hybrid-mesenchymal transitions (Figure SI1) receives a variety of signals, either inducing (eg. HIF1α, TGF-β, IGF, EGF, HGF) or repressing (eg. p53) EMT. EMT-inducing signals increase the expression of the EMT-TFs SNAIL and ZEB, while p53 activates the expression of miR-34 and miR-200, the gatekeepers of the epithelial phenotype (1). Also, these signals interact in complex ways, for example, TGF-β promotes the degradation of p53 by activating MDM2, which activates MDM2 and hence increases the degradation of p53 (2).
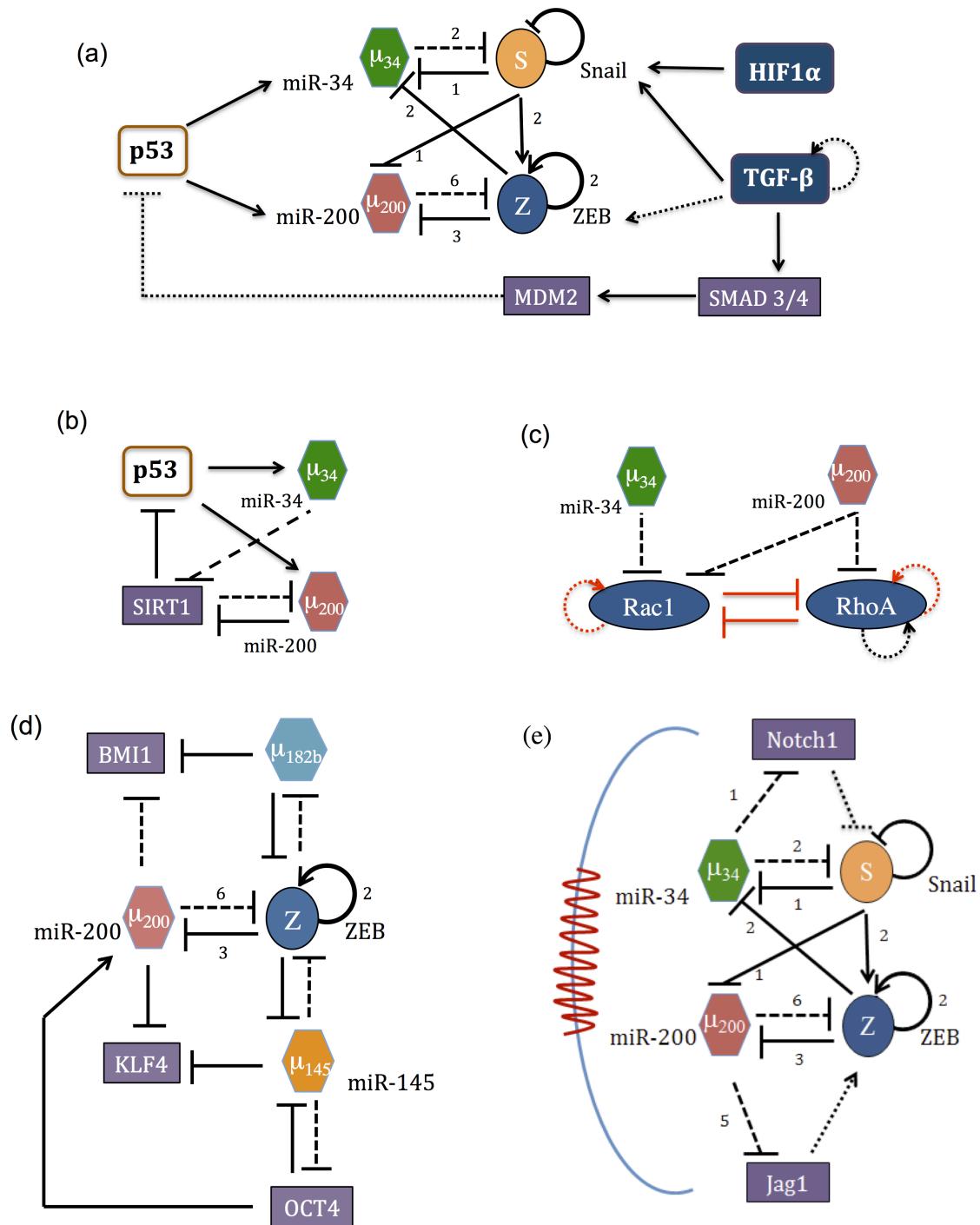
Fig SI1. EMT regulatory circuits are coupled to other key cellular signals. (a) p53 and TGF-β are opposing signals for EMT. TGF-β induces EMT by activating EMT-TFs; p53 inhibits EMT by inducing miRNAs. Also, TGF-β degrades p53 indirectly, through MDM2. (b) SIRT1 forms a toggle switch with miR-200, is inhibited by miR-34, and inhibits p53, thus effecting genome stability. (c) miR-34 and miR-200 inhibit Rac1 and RhoA, the two GTPases controlling cell motility. (d) miR-200 inhibits Jagged1, which in

turn upregulates ZEB. Also, miR-34 inactivates Notch, and Notch leads to degradation of SNAIL. Notch and Jag1 constitute an intricate pathway for cell-cell communication, as denoted by the red wave on the blue curve. Black arrows show transcriptional activation, black bars show transcriptional inhibition, Black dotted lines show indirect regulation, black dashed lines show miRNA-mediated translational inhibition, red solid bars show phosphorylation inhibition, red dotted arrows show direct or indirect phosphorylation activation.

In addition to its direct role in EMT, miR-200/ZEB regulates many other key cellular characteristics, sometimes in collaboration with miR-34. miR-200 forms a mutual inhibition loop with SIRT1 (3), a NAD-dependent deacetylase which not only coupled to genome stability through p53, but also is involved in a range of physiological functions including metabolism and aging (Fig SI1b). Also, miR-200 and miR-34 inhibit Rac1 and RhoA (4, 5) – two GTPases which govern the mode of cell motility – mesenchymal vs. amoeboid. This indicates that epithelial-hybrid-mesenchymal and mesenchymal-amoeboid transitions may be related (Fig SI1c) (6, 7).

Furthermore, miR-200 inhibits BMI1 and KLF4, two stemness-associated factors; and ZEB inhibits miR-145, which forms another double negative feedback loop with OCT4 (Fig SI1d) (8, 9). It has been shown that miR-200/ZEB does indeed regulate stemness – both during the generation of Cancer Stem Cells (CSCs) (10) and the reprogramming of fibroblasts to iPSCs (11). Besides, both modules of the core EMT circuit regulate and are regulated by the key cell-cell communication pathway involving Notch/Jagged1. miR-200 strongly inhibits Jagged1 (12), which induces ZEB expression (13). Also, miR-34a inhibits Notch1 expression (14), while Notch induces the degradation of SNAIL(15) (Fig SI1f). Consequently, miR-200/ZEB has been referred to as "motor of cellular plasticity" (16), especially during tumorigenesis, as it helps confer on tumor cells resistance to apoptosis, senescence and chemotherapy.

2. Consistency with experimental observations

Figure 1 is a schematic diagram of the EMT core regulatory network, which consists of two highly interconnected modules – miR-34/SNAIL and miR-200/ZEB mutually inhibitory chimeric circuits. In the miR-34/SNAIL loop, miR-34 has two binding sites on SNAIL 3' UTR, whereas SNAIL binds to a conserved site in promoter region of miR-34 (17). The miR-200 family is divided into two subgroups based on seed sequences – subgroup I: mir-141 and miR-200a, and subgroup II: miR-200b,c and miR-429. The ZEB1 3' UTR has eight miR-200 conserved binding sites (three for subgroup I, five for subgroup II), and ZEB2 3' UTR has nine of them (three for subgroup I, six for subgroup II). ZEB1 and ZEB2 (considered together as the ZEB family) bind to conserved sites in the promoter region of all miR-200 family members (18, 19). Since stable expression of miR-200c alone can restore E-cadherin expression (20), we considered in our model six binding sites of the miR-200 family to ZEB mRNA, and three binding sites on the miR-200 promoter from ZEB. Both ZEB and SNAIL bind to E-boxes in the relevant promoter regions (19). Also, SNAIL represses its own transcription (21), and activates ZEB (22). As the ZEB promoter has multiple E-boxes (23), and ZEB activates its transcription indirectly through stabilizing SMAD complexes (44), we assumed that ZEB activates itself by binding to two sites in its promoter region.

Using dynamical systems analyses, we show that miR-34/SNAIL chimeric circuit behaves as a noise-buffering integrator and miR-200/ZEB acts as the decision making module for cells to undergo partial or complete EMT (i.e. a transition to a hybrid state or a completely mesenchymal state). These theory-based findings are consistent with several experimental findings. For example, it has been shown that while activation of SNAIL can initiate the transcriptional repression of E-cadherin, ZEB1 is required for full inhibition (24), and hence for the completion of the Epithelial to Mesenchymal Transition (EMT). Similarly, it has been shown that a complete reversal to an epithelial phenotype requires a strong inhibition of ZEB1 (25), and conversely knockdown of SNAIL is not sufficient (26). Furthermore, once cells attain high ZEB levels, for example via an increase of TGF-β, they do not immediately revert to epithelial phenotype upon

subsequent removal of TGF-β. Cells with sufficiently low levels of ZEB do revert (27), indicating that the miR-200/ZEB module marks the commitment point for cells to undergo EMT. Also, most of the genes that are down-regulated during EMT are transcriptionally inhibited by ZEB1 (28), suggesting that indeed it is ZEB that acts as master regulator for EMT decision making.

3. Theoretical framework for microRNA-based chimeric circuits

In our recent study (29), we developed a new computational model for $\underline{m}$icroRNA-$\underline{b}$ased $\underline{c}$himeric (MBC) circuits. In MBC circuits, one or more microRNA (miR) molecules bind to the 3' UTR of an mRNA for the target protein to form a miR-mRNA complex. miRs can inhibit translation of mRNA and/or actively degrade mRNA, and can be degraded or recycled (30). In the MBC model, we capture all these features by explicitly modeling the various miR-mRNA complexes formed by the binding/unbinding chemical reactions of miR and mRNA (Fig 3 and Fig SI2).

Suppose an mRNA molecule has n miR binding sites. There are then a total of $n+1$ possible configurations of mRNA, each of which binds i miR molecules. Since a miR molecule is only 22 nt long, and recognizes mRNA by a seed sequence of 7-8 nt, we consider binding to be independent for the different miR binding sites. We refer to the binding rate as $r_{\mu+}$, the unbinding rate as $r_{\mu-}$, the miR concentration as μ, and the total mRNA concentration as m. We assume that the binding/unbinding rate of miR and mRNA is fast compared to the rates for molecule production/degradation. Then, at equilibrium, the concentration of mRNA $[m_i]$, where i miR binds specifically to i binding sites of mRNA, obeys

$$r_{\mu+}\mu[m_i] = r_{\mu-}[m_{i+1}]. \quad \text{(S1)}$$

We set $\mu_0 = r_{\mu-}/r_{\mu+}$, and therefore $[m_i] = (\mu/\mu_0)^i[m_0]$.

All terms $[m_i]$ should also satisfy

$$\sum_{i=0}^{n} C_n^i[m_i] = m. \quad \text{(S2)}$$

Here, C_n^i is the number of i-combinations of n items, defined as $\dfrac{n!}{i!(n-i)!}$, as there are C_n^i different mRNA configures when i out of n binding sites are occupied by miRs. So,

$$[m_i] = mM_n^i(\mu), \quad \text{(S3)}$$

where $M_n^i(\mu) = \dfrac{(\dfrac{\mu}{\mu_0})^i}{(1+\dfrac{\mu}{\mu_0})^n}$ (see Fig SI2).

Then, the total translation rate is

$$\sum_{i=0}^{n} l_i C_n^i [m_i] = m \sum_{i=0}^{n} l_i C_n^i M_n^i(\mu) = mL(\mu) ,$$

the total mRNA active degradation rate is

$$\sum_{i=0}^{n} \gamma_{mi} C_n^i [m_i] = m \sum_{i=0}^{n} \gamma_{mi} C_n^i M_n^i(\mu) = mY_m(\mu) ,$$

and the total miR active degradation rate is

$$\sum_{i=0}^{n} \gamma_{\mu i} C_n^i [m_i] = m \sum_{i=0}^{n} \gamma_{\mu i} C_n^i M_n^i(\mu) = mY_\mu(\mu) .$$

Here, l_i is the individual translation rate (normalized to one for the case of no miR inhibition), γ_{mi} and $\gamma_{\mu i}$ are the individual active degradation rates for mRNA and miR. Depending on the choice of the parameters (see the next section), the MBC model can capture different mechanisms of miR silencing; for example, one or multiple miRs can bind to an mRNA, and sequester the mRNA ($l_i < 1$) before the complex is eventually co-degraded(31)

Given the above, the deterministic equations of a circuit with miR μ, mRNA m and protein B is

$$\begin{aligned}
\dot{\mu} &= g_\mu - mY_\mu(\mu) - k_\mu \mu \\
\dot{m} &= g_m - mY_m(\mu) - k_m m , \qquad \text{(S4.1)} \\
\dot{B} &= g_B mL(\mu) - k_B B
\end{aligned}$$

where g_μ and g_m are the synthesis rates (possibly functions of B and external signals) of μ and m respectively, k_μ, k_m, k_B are the constant innate degradation rates of μ, m and B respectively, and g_B is the translation rate of protein B for each mRNA in the absence of miR. The corresponding deterministic equations for miR-200/ZEB circuit

$$\dot{\mu}_{200} = g_{\mu_{200}} H^S(Z, \lambda_{Z,\mu_{200}}) H^S(S, \lambda_{S,\mu_{200}}) - m_Z Y_\mu(\mu_{200}) - k_{\mu_{200}} \mu_{200}$$
$$\dot{m}_Z = g_{m_Z} H^S(Z, \lambda_{Z,m_Z}) H^S(S, \lambda_{S,m_Z}) - m_Z Y_m(\mu_{200}) - k_{m_Z} m_Z \qquad , \qquad \text{(S4.2)}$$
$$\dot{Z} = g_Z m_Z L(\mu_{200}) - k_Z Z$$

miR-34/SNAIL circuit
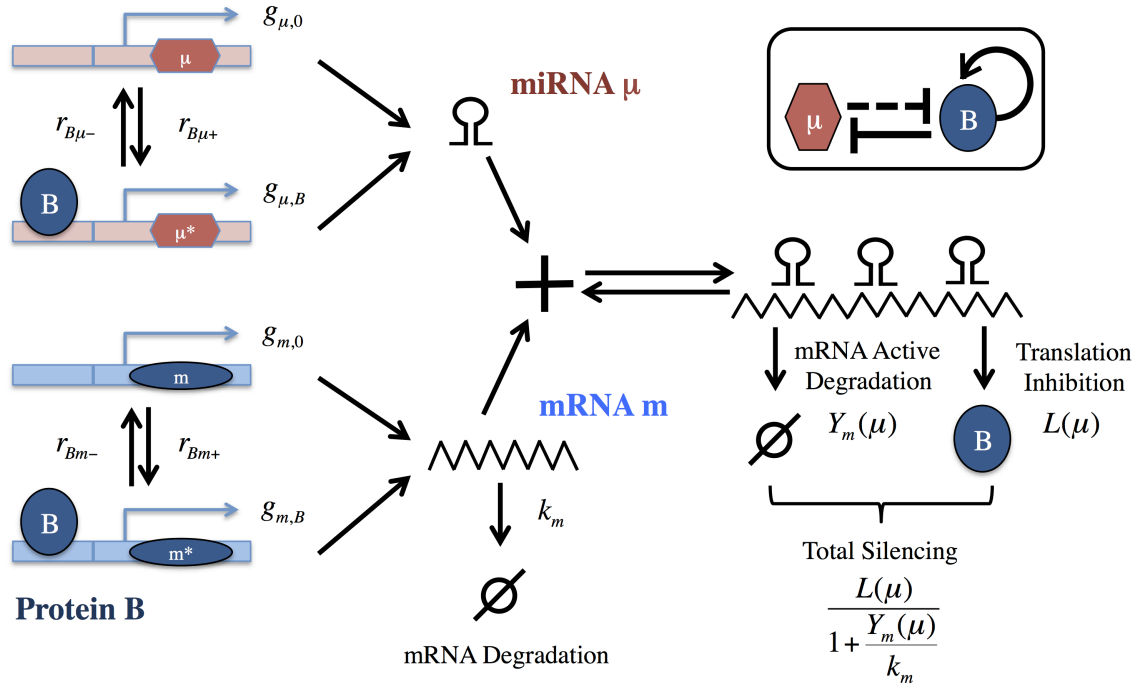
$$\dot{\mu}_{34} = g_{\mu_{34}} H^S(S, \lambda_{S,\mu_{34}}) - m_S Y_\mu(\mu_{34}) - k_{\mu_{34}} \mu_{34}$$
$$\dot{m}_S = g_{m_S} H^S(S, \lambda_{S,m_S}) H^S(I, \lambda_{I,m_S}) - m_S Y_m(\mu_{34}) - k_{m_S} m_S \qquad , \qquad \text{(S4.3)}$$
$$\dot{S} = g_S m_S L(\mu_{34}) - k_S S$$

combined circuit

$$\dot{\mu}_{200} = g_{\mu_{200}} H^S(Z, \lambda_{Z,\mu_{200}}) H^S(S, \lambda_{S,\mu_{200}}) - m_Z Y_\mu(\mu_{200}) - k_{\mu_{200}} \mu_{200}$$
$$\dot{m}_Z = g_{m_Z} H^S(Z, \lambda_{Z,m_Z}) H^S(S, \lambda_{S,m_Z}) - m_Z Y_m(\mu_{200}) - k_{m_Z} m_Z$$
$$\dot{Z} = g_Z m_Z L(\mu_{200}) - k_Z Z$$
$$\dot{\mu}_{34} = g_{\mu_{34}} H^S(S, \lambda_{S,\mu_{34}}) H^S(Z, \lambda_{Z,\mu_{34}}) - m_S Y_\mu(\mu_{34}) - k_{\mu_{34}} \mu_{34} \qquad , \qquad \text{(S4.4)}$$
$$\dot{m}_S = g_{m_S} H^S(S, \lambda_{S,m_S}) H^S(I, \lambda_{I,m_S}) - m_S Y_m(\mu_{34}) - k_{m_S} m_S$$
$$\dot{S} = g_S m_S L(\mu_{34}) - k_S S$$

where H^S is the shifted Hill function, defined as $H^S(B,\lambda) = H^-(B) + \lambda H^+(B)$, $H^-(B) = 1/[1 + (B/B_0)^{n_B}]$, $H^+(B) = 1 - H^-(B)$ and λ is the fold change from the basal synthesis rate due to protein B. $\lambda > 1$ for activators, while $\lambda < 1$ for inhibitors. In equation (S4.2), the SNAIL level S serves as the external input signal for the miR-200/ZEB circuit.

(a)

$g_{\mu,0}$

$r_{B\mu-}$ $r_{B\mu+}$

μ

μ^*

$g_{\mu,B}$

B

miRNA μ

μ ⊣ ⊣ B

$g_{m,0}$

r_{Bm-} r_{Bm+}

m

m^*

B

$g_{m,B}$

mRNA m

Protein B

k_m

∅

mRNA Degradation

+

mRNA Active Degradation

∅ $Y_m(\mu)$

Translation Inhibition

B $L(\mu)$

Total Silencing

$$\frac{L(\mu)}{1+\dfrac{Y_m(\mu)}{k_m}}$$

(b)

	Population	Degeneracy	Effective Translation	mRNA Active Degradation	microRNA Active Degradation
	$M_n^0(\mu)$	C_n^0	l_0	0	0
	$M_n^1(\mu)$	C_n^1	l_1	γ_{m1}	$\gamma_{\mu1}$
	$M_n^2(\mu)$	C_n^2	l_2	γ_{m2}	$\gamma_{\mu2}$
⋮			⋮		
	$M_n^i(\mu)$	C_n^i	l_i	γ_{m2}	$\gamma_{\mu2}$
⋮					
Total			$\sum\limits_{i=0}^{n} l_i C_n^i M_n^i$	$\sum\limits_{i=1}^{n} \gamma_{mi} C_n^i M_n^i$	$\sum\limits_{i=1}^{n} i\gamma_{\mu i} C_n^i M_n^i$

Fig SI2. Schematic diagrams of the MBC model. (a) Illustration of the MBC model for the self-activating chimeric toggle switch (μ-m). This is similar to Fig 3 in the main text, except that the transcriptional regulations in the circuit are also explicitly presented. (b) Quantitative description of miR-mediated translation silencing. The leftmost column shows the illustrations of various miR-mRNA complexes. In the ith row, $i+1$ binding sites are occupied by miR molecules. The second column from the left shows the population of each configuration at binding/unbinding equilibrium. The third column shows the degeneracy of each configuration. The fourth to sixth columns show the notations for the individual translation rate, mRNA degradation and miR degradation. The overall effects obtained by summing over all configurations are listed in the last row.

4. Parameter estimation for the MBC ciruits

In the MBC model, there are parameters of translation rates and active degradation rates for each miR-mRNA configuration. Here we discuss we selected the parameters so as to match translation silencing effects from the experiment.

Consider a gene B with constant transcription rate g_m, giving the deterministic equations for both mRNA m and protein B as

$$\dot{m} = g_m - k_m m$$
$$\dot{B} = g_B m - k_B B$$

At equilibrium, the concentration of protein B_0 should be

$$B_0 = \frac{g_B g_m}{k_Z k_m}.$$

Similarly, if the same gene B is inhibited by miR with concentration μ,

$$\dot{m} = g_m - m Y_m(\mu) - k_m m$$
$$\dot{B} = g_B m L(\mu) - k_B B$$

At equilibrium, the concentration of protein B will be

$$B = \frac{g_B g_m L(\mu)}{k_B(k_m + Y_m(\mu))}.$$

We define $P(\mu)$ as B divided by B_0, to represent the fold change of translation in the presence of miR.

$$P(\mu) = \frac{B}{B_0} = \frac{L(\mu)}{1 + \frac{Y_m(\mu)}{k_m}} \quad (S5)$$

Typical values of P range from 0 for complete silencing, to 1 for no silencing (see Fig SI3), depending on μ and the number of binding sites of miR on the 3'UTR of target mRNA. This result shows that the overall silencing is due to the combined effect of both miR-mediated inhibition of the translation process and miR-assisted active degradation of the mRNAs. The lower the L function and/or the higher the Y_m function, the larger is the overall silencing effect.

In the MBC model, we specifically chose the parameters l_i and γ_{mi} to match the value of $P(\mu)$ at the threshold $\mu=\mu_0$ to the experimental data. Experiments on (miR-34/SNAIL) show that SNAIL levels go down to around 80% of baseline when miR-34 binds to one binding site on SNAIL mRNA, and about 50% when miR-34 binds to both of them (32). Also, miR-200 brings down ZEB levels to 10% baseline with six binding sites (33).

To make the parameters more reliable, we constrained the parameter space according to the following rules. First, $l_0 = 1$ and $\gamma_{m0} = 0$, as there should be no silencing effect when no miR is bounded. Second, $l_0 \geq l_1 \geq ... \geq l_n$, $\gamma_{m0} \geq \gamma_{m1} \geq ... \geq \gamma_{mn}$, to account for stronger silencing effects when more miRs are bounded. Third, l_n is not necessarily close to zero, so the model can allow for some leakage translation. Moreover, we made an assumption that the translation/degradation rates saturate once the mRNA contains more than certain number (3 or 4 in this study) of miRs.

Since different miRs adopt different mechanisms for silencing (34), we tested a total of five versions of the parameters, as listed in Table SI1. In the first case, only the translation inhibition was considered (denoted as "L Only").; hence $\gamma_{mi} = 0$, $P(\mu) = L(\mu)$. In the second case, only the mRNA active degradation was considered (denoted as "Y Only"; hence $l_i = 0$, $P(\mu) = 1/(Y_m(\mu)/k_m + 1)$. For the third to the fifth cases, both effects were considered, but with different weights. In third case, the magnitude of $L(\mu)$ is similar to that of $1/(Y_m(\mu)/k_m + 1)$ (denoted as "Both, equal"). In the fourth case, $L(\mu)$ is dominant (denoted as "Both, L stronger"); and finally, in the last case, $1/(Y_m(\mu)/k_m + 1)$ is dominant (denoted as "Both, Y stronger"). It should be noted that the parameters γ_{mi} depends on k_m, which was set as 0.5 Hour^{-1} for both ZEB and SNAIL in this study (See section 5 for more details).

As shown in Fig SI3, all sets of parameters mentioned above give similar $\mu - P$ curves for the same number of miR binding sites. For different number of binding sites, $P(\mu_0)$ is about 0.75, 0.5, 0.1 and 0.1 for n equals to 1, 2, 5 and 6 respectively, which matches

well with the experiments mentioned above. Although the mechanism of silencing is not the same in each version, the "total silencing" effect, as characterized by $P(\mu)$, is similar. Depending on the detailed silencing mechanism of the miRs in a specific circuit, one of the parameter versions might be more suitable for modeling the dynamics. We will discuss the behavior of the miR-200/ZEB circuit for different versions of parameters in section 6.

Since the term $Y_\mu(\mu)$ does not appear in $P(\mu)$, the parameters $\gamma_{\mu i}$ are not constrained by total silencing results. In this study, we chose $\gamma_{\mu i}$ to be smaller than γ_{mi}, because active degradation of mRNA is known to be higher than that of miR. The values $\gamma_{\mu i}$ are the same for different versions of parameters, and they are listed in the last row in Table SI1.

We also numerically compared the magnitude of active degradation and innate degradation for both miR and mRNA, as shown in Table SI2. The innate degradation rate for miR $k_{\mu_{200}}$ is set as 0.05 Hour^{-1} for all cases (see section 6). We mainly tested the values of $\mu_{200}k_{\mu_{200}}$, $m_Z Y_\mu$, $m_Z k_{m_Z}$ and $m_Z Y_{m_Z}$ for the three states (the three stable steady states of the miR-200/ZEB module, as shown in Fig 3 in the main article). With the current parameters, the miR active degradation level is similar or less than the innate degradation level, depending on the mRNA level.

Conversely, the mRNA active degradation level is mostly higher than the innate degradation level when the miR level is at or above the threshold μ_0.

n (# of miR binding sites)		0	1	2	3	4	5	6
L Only	l_i	1.0	0.5	0.2	0.02	0.02	0.02	0.02
Y Only	γ_{mi} (Hour^{-1})		0.3	1.5	7.5	7.5	7.5	7.5
Both,	l_i	1.0	0.7	0.5	0.1	0.05	0.05	0.05
equal	γ_{mi} (Hour^{-1})		0.1	0.5	2.5	2.5	2.5	2.5
Both,	l_i	1.0	0.6	0.3	0.1	0.05	0.05	0.05
L stronger	γ_{mi} (Hour^{-1})		0.04	0.2	1.0	1.0	1.0	1.0
Both,	l_i	1.0	0.8	0.6	0.3	0.1	0.1	0.1
Y stronger	γ_{mi} (Hour^{-1})		0.15	0.75	4.0	4.0	4.0	4.0
---	$\gamma_{\mu i}$ (Hour^{-1})		0.005	0.05	0.5	0.5	0.5	0.5

Table SI1. Parameters of l_i, γ_{mi} and $\gamma_{\mu i}$ for various cases. "L Only" is the case when only translation inhibition is considered. "Y Only" is the case when only active mRNA degradation is considered. "Both" denote the cases when both mechanisms are considered, but with different weights. The parameters are set so that the total silencing for each case is similar to the experimental data. The parameters highlighted in light blue are the ones primarily used in our modeling effort.

States (Molecules)	m_{200}: 1.71 K m_z : 827 Z : 564.7 K	m_{200}: 11.69 K m_z : 326 Z : 52.4 K	m_{200}: 18.67 K m_z : 66 Z : 6.46 K
m_{200} Innate Degradation (K Molecules/Hour)	0.086	0.585	0.933
m_{200} Active Degradation (K Molecules/Hour)	0.073	0.459	0.122
m_z Innate Degradation (K Molecules/Hour)	0.414	0.163	0.033
m_z Active Degradation L ~ Y (K Molecules/Hour)	0.195	0.626	0.149
m_z Active Degradation L < Y (K Molecules/Hour)	0.302	0.999	0.238
m_z Active Degradation L > Y (K Molecules/Hour)	0.078	0.251	0.059

Table SI2. Comparison of the degradation levels in the miR-200/ZEB circuit for the various stable steady states. There are six miR-200 binding sites on the ZEB mRNA. The m_{200} innate degradation is computed by $\mu_{200}k_{\mu_{200}}$, the m_{200} active degradation by $m_z Y_\mu$, the m_z innate degradation by $m_z k_{m_z}$ and the m_z active degradation by $m_z Y_{m_z}$.
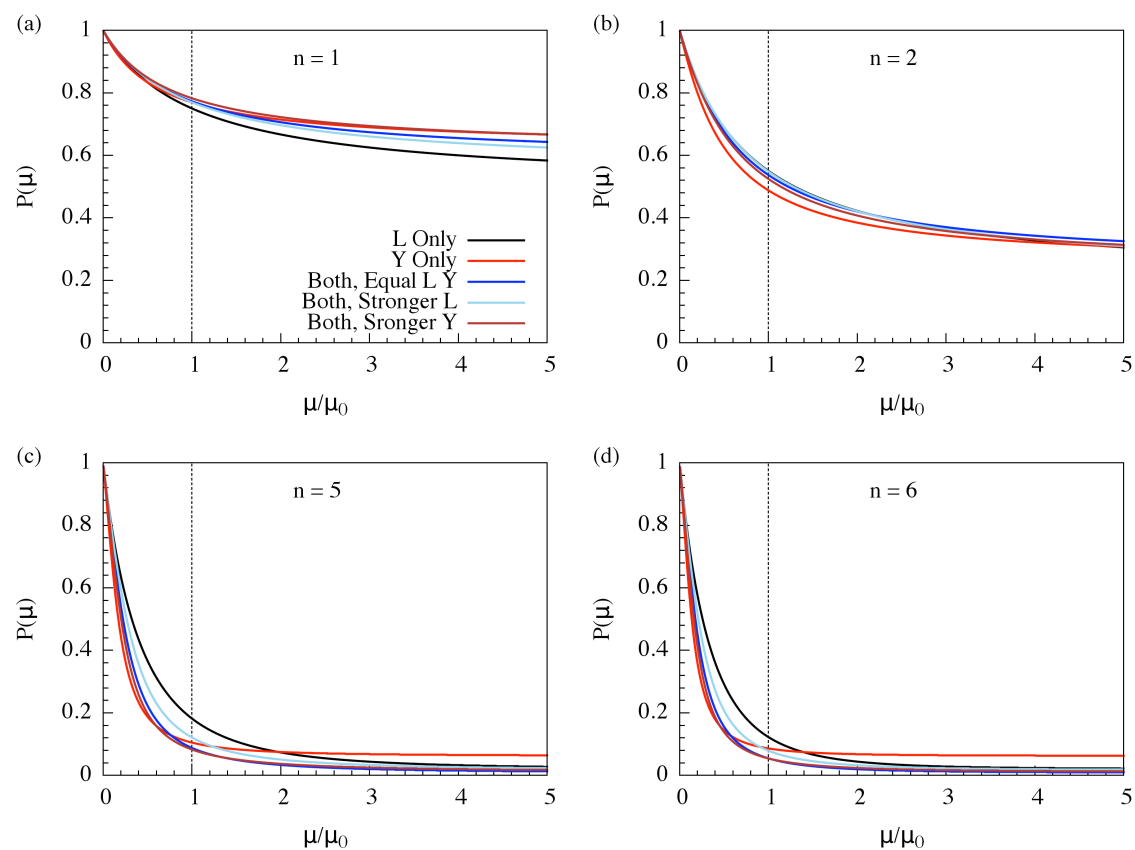
Fig SI3. The magnitude of $P(\mu)$ for the different versions of parameters. An individual graph contains five curves, each of which correspond to a version whose parameters are listed in Table SI1. a) one miR binding site; b) two binding sites; c) five binding sites; d) six binding sites. The vertical lines indicate the values of $P(\mu)$ at the miR threshold concentration μ_0.

5. Multi-stability of miR-based chimeric (MBC) toggle switches

Many studies demonstrate multi-stability of transcription-factor-only toggle switch circuits (35). Typically, toggle switches with nonlinear mutual repression can be bistable. In this section, we check the multi-stability of chimeric (involving both miRNA's and TF's)_toggle switches.

Consider a generic chimeric toggle switch circuit, which is composed of a single miR μ and a single transcription factor B. The deterministic equations for the MBC model is

$$\dot{\mu} = g_{\mu}H^{S}(B, \lambda_{B,\mu}) - mY_{\mu}(\mu) - k_{\mu}\mu$$
$$\dot{m} = g_{m}H^{S}(B, \lambda_{B,m}) - mY_{m}(\mu) - k_{m}m, \quad (S6)$$
$$\dot{B} = g_{B}mL(\mu) - k_{B}B$$

where $H^{S}(B, \lambda_{B,\mu})$ is the shifted Hill function for transcriptional regulation by the protein B, $H^{S}(B, \lambda_{B,\mu})$ arises via auto-regulation of protein B, and λ is the fold change of the transcription rate by protein B. $H^{S}(B, \lambda) = H^{-}(B) + \lambda H^{+}(B)$, $H^{-}(B) = 1/[1 + (B/B_{0})^{n_{B}}]$ and $H^{+}(B) = 1 - H^{-}(B)$. For a toggle switch, $\lambda_{B,\mu} < 1$, representing B's repression to μ's transcription.

As the innate degradation rate of the mRNA is about five to ten times faster than those of the miR and the protein (36), we assume that the mRNA can rapidly reach equilibrium before substantial changes of the miR and the protein levels. So, we set

$$m = \frac{g_{m}}{k_{m}}\frac{k_{m}H^{S}(B, \lambda_{B,m})}{Y_{m}(\mu) + k_{m}} = g'_{m}\frac{k_{m}H^{S}(B, \lambda_{B,m})}{Y_{m}(\mu) + k_{m}}, \quad Q(\mu) = \frac{k_{m}Y_{\mu}(\mu)}{k_{\mu}[Y_{m}(\mu) + k_{m}]},$$

and from equation (S6),

$$\dot{\mu} = g_{\mu}H^{S}(B, \lambda_{B,\mu}) - k_{\mu}g'_{m}H^{S}(B, \lambda_{B,m})Q(\mu) - k_{\mu}\mu$$
$$\dot{B} = g_{B}g'_{m}H^{S}(B, \lambda_{B,m})P(\mu) - k_{B}B \quad . \quad (S7)$$

Thus, we obtain the reduced MBC model. In the following, we will use it to analyze the multistability of the circuit. Compared to the equations for transcription-factor-only circuits, the protein equation differs in the synthesis term, where the term

$H^S(B,\lambda_B)H^S(A,\lambda_A)$ is replaced by $H^S(B,,\lambda_B)P(\mu)$. However, the miR equation contains an additional term that includes the $Q(\mu)$ function, which adds more nonlinearity.

# of m Binding Sites	P Formulae	a/μ_0	b (b > 0)
1	$P(\mu) = \dfrac{1-b}{1+\dfrac{\mu}{a}} + b$	0.93	0.56
2		0.78	0.20
5	$P(\mu) = \dfrac{1-b}{(1+\dfrac{\mu}{a})^2} + b$	0.58	0.004
6		0.45	0.002

Table SI3. Nonlinear fitting of the P function for various numbers of miR binding sites. For the case of one or two binding sites, the $\mu - P$ curve is fit to the rank-one inhibitory Hill function; for the case of five or six binding sites, the $\mu - P$ curve is fit to $(1+\dfrac{\mu}{a})^{-2}$.

The parameter set "Both, L stronger" was chosen for the fitting.
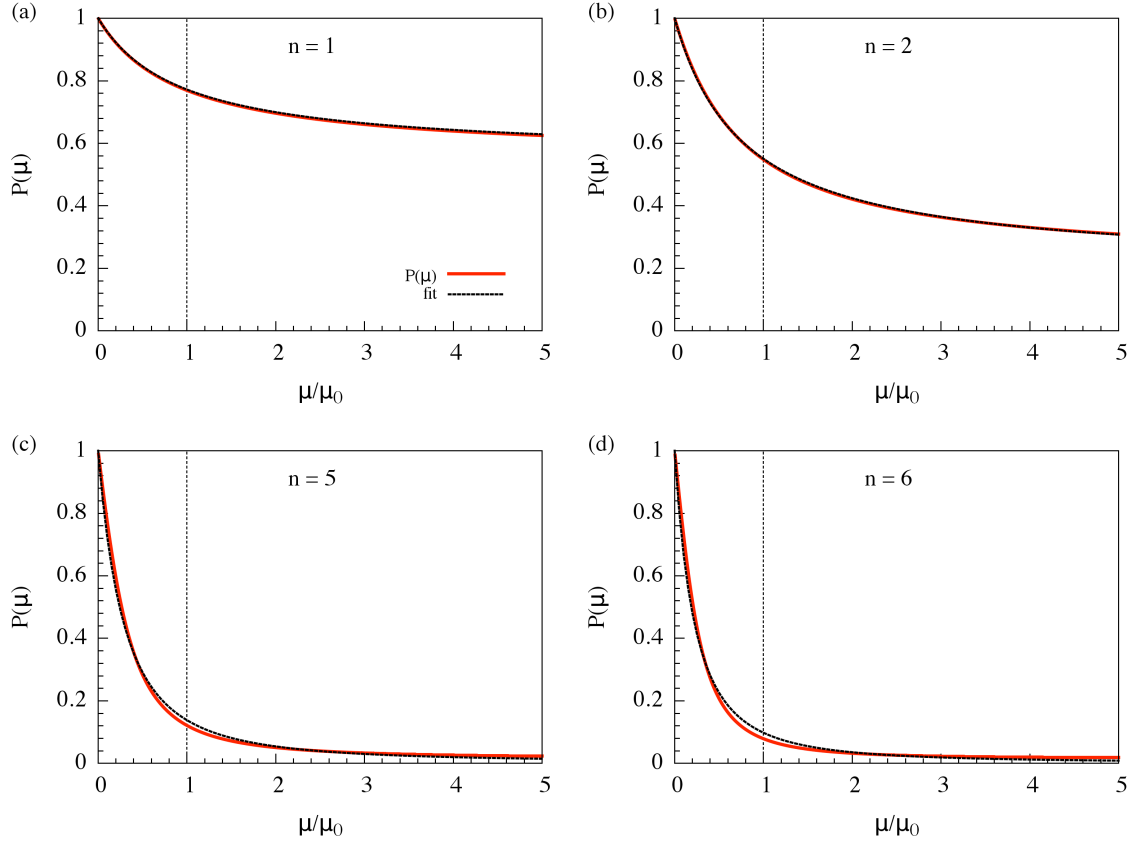
Fig SI4. Numerical fitting of the P function for various numbers of miR binding sites. Nonlinear fitting was performed for the P function, as shown in Table SI3. Here is shown the comparison of the P function (red solid lines) with the fitted curve (black dotted lines). a) one binding site; b) two binding sites; c) five binding sites; d) six binding sites. Better fitting was achieved when the number of binding sites is low, because of weak nonlinearity.
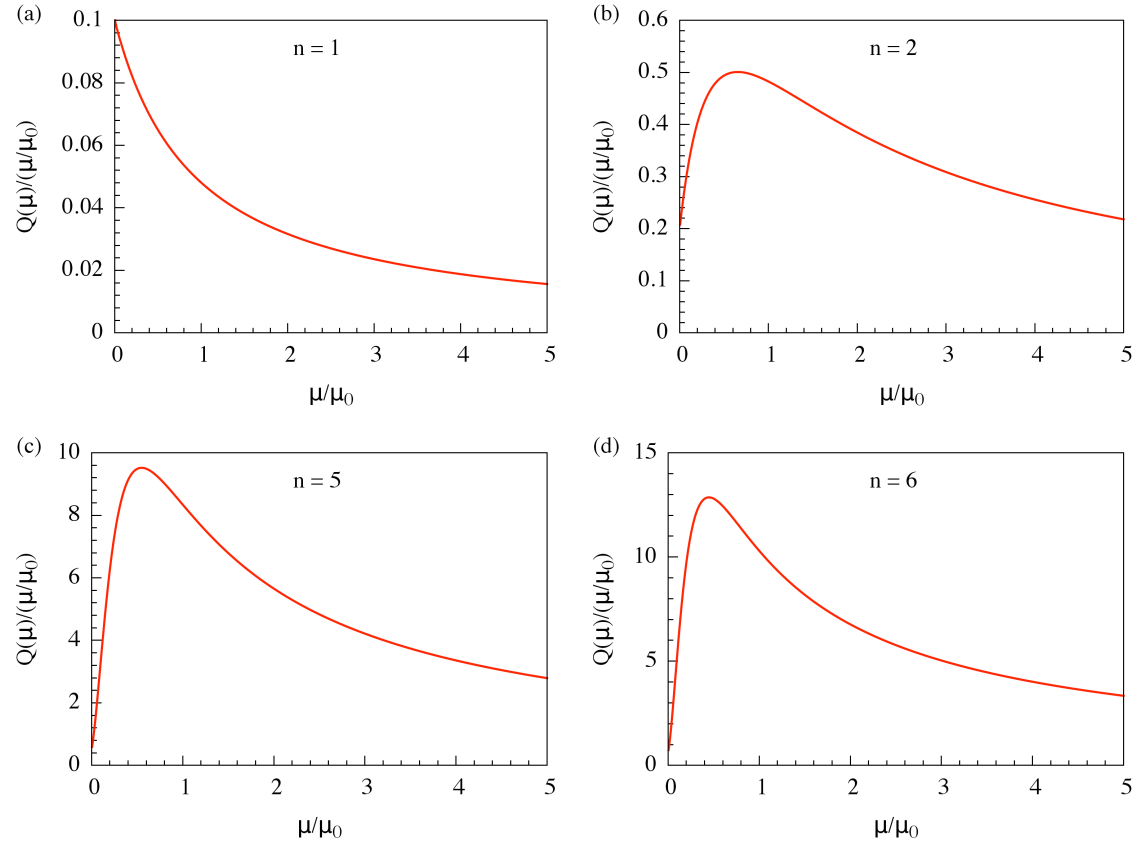
Fig SI5. The Q function for various numbers of miR binding sites. The y-axes are the values of Q function normalized by μ/μ_0. a) one binding site; b) two binding sites; c) five binding sites; d) six binding sites. The magnitude of Q increases when the number of binding sites increases.

Next, the P functions for various numbers of binding sites were fitted to some nonlinear functions (see Table SI3 for the formulae and parameters, Fig SI4 for the actual fitting). The results show that the P function fits nicely to the rank-one inhibitory Hill function, when there is one or two miR binding sites. But the fit is not acceptable for the case of five or six binding sites, as the P function has more nonlinearity. Instead, the P function is close to the form of $(1+\frac{\mu}{a})^{-2}$; It does not take the shape of a Hill function with high order.

For the Q function, there exists a maximum at around $\mu = 0$ for $n = 1$, and at around $\mu = 0.5\ \mu_0$ for $n > 1$. The value at the maximum dramatically increases when n increases. For $n = 1$ or 2, $Q(\mu) < 0.5\mu / \mu_0$. In this study, $\mu_0 = 10$ K molecules, and the maximum number of mRNA is about 1K molecules (see Fig SI11). Because of the self-inhibition of protein B, $g'_m H^S(B,\lambda_{B,m}) \le \dfrac{g_m}{k_m} \sim 1$ K molecules. Therefore,

$$k_\mu g'_m H^S(B,\lambda_{B,m})Q(\mu) \le 0.05 k_\mu \mu .$$

Hence, the active miR degradation term is small compared to the innate miR degradation term. By omitting the active term, the equations for $n = 1$ or 2 become

$$\begin{aligned} \dot{\mu} &\approx g_\mu H^S(B,\lambda_{B,\mu}) - k_\mu \mu \\ \dot{B} &= g_B g'_m H^S(B,\lambda_{B,m})P(\mu) - k_B B \end{aligned}, \quad \text{(S8)}$$

where $P(\mu) = \dfrac{1-b}{1+\dfrac{\mu}{a}} + b$.

If the circuit does not have auto-regulation, $H^S(B,\lambda_{B,m}) = 1$. The fixed point(s) (μ, B)

satisfies $\dfrac{\alpha}{1+(\dfrac{B}{B_0})^{n_B}} + \beta = \mu$, and $(\dfrac{B}{B_0})^{n_B} = \gamma[P(\mu)]^{n_B}$. And finally,

$$\frac{\alpha/\gamma}{\mu-\beta} - \frac{1}{\gamma} = [P(\mu)]^{n_B} \quad , \quad \text{(S9)}$$

In Figure S6, we plotted the function $0.5/(\mu-1)$ (black solid lines) as an example of the left hand side of equation (S9) (without the constant shift). The curve is also superimposed with the P^{n_B} curves of different n_B to represent possible right hand sides. As shown in Figure S6a, when $n = 1$, there is never more than one fixed point. So the switch is monostable. When $n = 2$, $n_B \leq 3$, there is also just one fixed point. But it is possible to have three fixed points, starting from $n_B \geq 4$. So, the switch becomes bistable for certain range of parameters.

If the circuit has auto-regulation, $H^S(B, \lambda_{B,m}) \neq 1$. If the type of auto-regulation is self-inhibition with Hill coefficient (rank) one, the second equation for the fixed point becomes $B/H^S(B, \lambda_{B,m}) = c[P(\mu)]$. Suppose $H^S(B, \lambda_{B,m}) \sim 1/[1 + \dfrac{B}{B_1}]$,

$B/B_1 \sim [0.25 + c'P(\mu)]^{1/2} - 0.5 \sim [c'P(\mu)]^{1/2}$, if $c' \gg 1$. So, equation (S10)

becomes $\dfrac{\alpha/\gamma'}{\mu - \beta} - \dfrac{1}{\gamma'} = [P(\mu)]^{n_B/2}$. Yet, no matter whether $c' \gg 1$ or not, the right hand side

of equation (S10) drops more slowly than that for the case without self-inhibition. Therefore, self-inhibition makes it harder for the switch to exhibit bistability.

The above analysis is consistent with our numerical results for the miR-34/SNAIL circuit module, where SNAIL mRNA contains only two miR-34 binding sites, miR-34 promoter has one binding site for SNAIL, and SNAIL self-inhibits transcriptionally with rank one. Our analysis shows that the circuit can only be monostable, rather than being bistable as would be expected for a generic toggle switch involving only transcription factors.

The analysis is also consistent with the numerical results of the model circuit presented in our previous study (29), where the mRNA of the protein B contains six binding sites of miR μ, and the μ's promoter has two binding sites for protein B. Both the theory here and our previous numerical results show that the circuit can be bistable (without auto-regulation).

When $n = 5$ or 6, the inhibition effect of the P function is stronger, and more nonlinear. Also, the miR active degradation term cannot be omitted anymore. Although it becomes tedious to fully analyze this system, intuitively, it should be easier, or the parameter space is larger, for the toggle switch circuit to have multistability. The miR-200/ZEB circuit module belongs to this case.
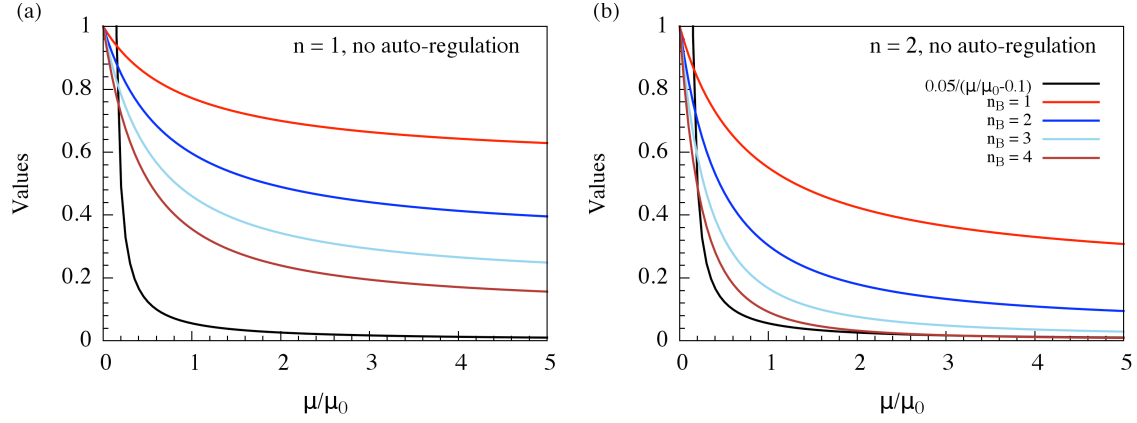

Fig SI6. State estimation for the miR-TF toggle switch circuit. The solid lines show the $0.5/(\mu - 1)$ curve, representing the left hand side of equation (S9). The colored lines show P^{n_B} curves, to represent the right hand side of equation (S9) for different n_B values. a) one miR binding site, and only monostable states are possible; b) two miR binding sites, bistable states are possible.

6. Additional Parameter Selection for the Circuits

In section 4, the parameters for the MBC model have been listed. Here, we will explain how we selected the other parameters, and how we tested different versions of the MBC parameters for the miR-200/ZEB circuit.

The innate degradation rates for the proteins, mRNAs and miRs were selected according to the half-lives of each molecule from experimental data. Since the typical half-life of mammalian proteins is about 10 hours (37), we chose 0.1 Hour^{-1} as the degradation rate for ZEB, and 0.125 Hour^{-1} for SNAIL. That of SNAIL is larger, because SNAIL is less stable (24). The half-lives of mRNA is roughly a few Hours (38), so we chose 0.5 Hour^{-1} as the innate degradation rate for the mRNA of both ZEB and SNAIL. As miR is generally more stable than mRNA (39, 40), the innate degradation rates of miR for both miR-200 and miR-34 were selected as 0.05 Hour^{-1}.The number of miR binding sites on different types of mRNA and the number of binding sites of ZEB and SNAIL on miR-34 and miR-200 are taken from experiment, as explained in detail in the main text and SI section 2.

The expression levels for various molecules were estimated according to the typical protein concentration and characteristic cell dimensions for eukaryotic cells, and were converted to the number of molecules. The length scale of a typical eukaryotic cell is about 10μm, and the characteristic concentration for a signaling protein is about 10nM to 1μM (41) So for a 1μM protein, the number of proteins is $\dfrac{6\times10^{23}\times10^{-6}}{10^{-3}}(10\times10^{-6})^{3}$, which is roughly one million molecules. Moreover, the ratio of protein/mRNA numbers for a gene is about 2800 (42), so the number of mRNA for a gene should be around 1000 molecules. On the other hand, the number of molecules for a microRNA is about ten thousand (43). In this study, we used "K molecules" as the unit for the number of molecules for proteins and miRs, and "molecules for mRNAs. The transcription rates for different molecules were chosen accordingly, so that the molecule levels are consistent

with the aforementioned expectations. The translation rate for a gene is about 140 proteins per mRNA per hour (42), so we used 0.1 K proteins per mRNA per hour.

Also for transcriptional regulation, the changes in synthesis rates from baseline were set to be about five to ten fold, i.e. the λ for activator ranges from 5 to 10, the λ for repressor from 0.1 to 0.2. The full list of parameters is listed in Table SI4.

We tested all five versions of parameters for the MBC model (Table SI1) of the (miR-200/ZEB) circuit (parameters in Table SI4b). By slightly adjusting a few parameters (Table SI4a), we managed to find tristability when both translation inhibition and active mRNA degradation are included (Fig SI7d, e, f). But the three stable steady states can be best characterized only when the translation inhibition has dominant role in the silencing effect (Fig SI7e). For the two cases when only one silencing mechanism is presented, we could only get at most bistability (Fig SI7b, c). Hence, the different silencing mechanisms could affect the multistability of the miR-involved toggle switch circuits. It would be interesting to explore the roles of these different mechanisms experimentally through mutational studies.

(a) Parameters for the MBC model

	L Only	Y Only	L ~ Y	L > Y	L < Y
$g_{\mu 200}$ (Molecules/Hour)	1.5K	1.5K	2.9K	2.1K	1.55K
g_{mZ} (Molecules/Hour)	12.5	15	30	11	20
$Z^0_{\mu 200}$ (Molecules)	200K	200K	300K	220K	250K
Z^0_{mZ} (Molecules)	50K	50K	30K	25K	50K

(b) Parameters for the miR-200/ZEB circuit

			Hour^{-1}		Molecules		
$n_{Z,\mu200}$	3	$\lambda_{Z,\mu200}$	0.1	$k_{\mu200}$	0.05	$S^0_{\mu200}$	180K
$n_{Z,mZ}$	2	$\lambda_{Z,mZ}$	7.5	k_{mZ}	0.5	S^0_{mZ}	180K
$n_{\mu200}$	6	$\lambda_{S,\mu200}$	0.1	k_Z	0.1	S	200K
$n_{S,\mu200}$	2	$\lambda_{S,mZ}$	10.0	g_Z	0.1K	μ^0_{200}	10K
$n_{S,mZ}$	2						

(c) Parameters for the miR-34/SNAIL circuit

			Hour^{-1}		Molecules		Molecules/Hour	
$n_{S,\mu34}$	1	$\lambda_{S,\mu34}$	0.1	$k_{\mu34}$	0.05	$S^0_{\mu34}$ 300K	g_{mS}	90.0
$n_{S,mS}$	1	$\lambda_{S,mS}$	0.1	k_{mS}	0.5	S^0_{mS} 200K	$g_{\mu34}$	1.35K
$n_{\mu34}$	2	$\lambda_{Z,\mu34}$	0.2	k_S	0.125	$Z^0_{\mu34}$ 600K		
n_I	2	$\lambda_{I,mS}$	10.0	g_S	0.1K	μ^0_{34} 10K		
						I^0_{mS} 50K		

Table SI4. List of parameters used in the simulations. The parameters highlighted in color are the ones fixed in our model calculations. The parameters in (a) are the only adjustable parameters for different versions of the MBC model. They were applied to test the multi-stability of the miR200-ZEB circuit (See Fig SI7).
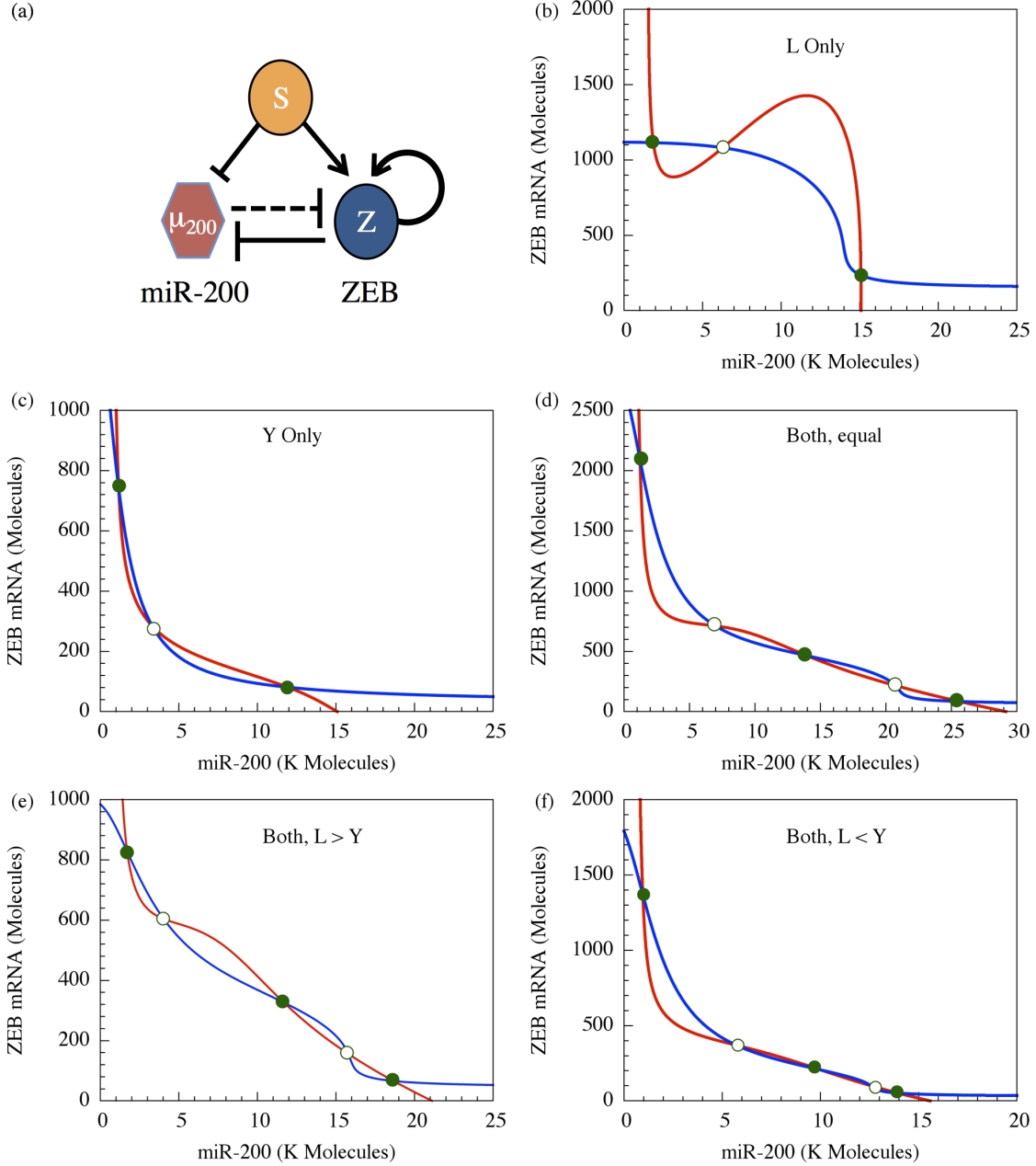
Fig SI7. Stable states of the (miR-200/ZEB) circuit for different parameters of the MBC model. a) Illustration of the (miR-200/ZEB) circuit., with SNAIL serving as the input signal. The model parameters are in Table SI1 and Table SI4. b) – f) show the nullclines of the system for different parameters of the MBC model. The red line is the nullcline for $d\mu_{200}/dt = 0, dZ/dt = 0$, and the blue line is the nullcline for $dm_Z/dt = 0, dZ/dt = 0$. The green solid points denote stable fixed points, and the green unfilled circles denote unstable/saddle fixed points. The parameters are the same as those listed in Table SI1 and Fig SI3.

7. The effects of signal noise on SNAIL

Here, we simulated the dynamics of the circuits with the presence of the external noise in the signal I. To simulate the external noise, the signal I follows the stochastic differential equation

$$\dot{I} = \alpha(I_0 - I) + \eta(t), \quad (S10)$$

where $<\eta(t), \eta(t')> = \Gamma\delta(t-t')$. I_0 is set to be 50 K molecules, α to be 0.04 hour^{-1}, and Γ to be 16 (K molecules/hour)^2. So $\bar{I} = I_0$ = 50 K molecules, $\sigma_I = \sqrt{\Gamma/(2\alpha)} \sim 14$ K molecules, and $<\Delta I(0)\Delta I(t)> = \sigma_I^2 \exp(-t/\tau)$, $\tau = 1/\alpha$ = 25 hours.

In our test, we take this noisy signal as an input for the miR-34/SNAIL circuit, and determined the corresponding variations in SNAIL level. First, the noisy signal is used as an input to miR-34 (I as transcription factor). According to the upper panels of Fig SI12, the self-inhibition of SNAIL reduces the variation of the SNAIL level (black line). Second, the noisy signal is taken as direct input to the SNAIL. From the bottom panels of Fig SI12, the self-inhibition of SNAIL again reduces the variation of the SNAIL level smaller (black line). In the absence of SNAIL self-inhibition, the variability of SNAIL is independent of the presence (red line) or absence (blue line) of coupling to miR-34.

Thus, the self-inhibition of SNAIL may serve as a filter of the external noise, and thus prevent the aberrant activation of EMT.
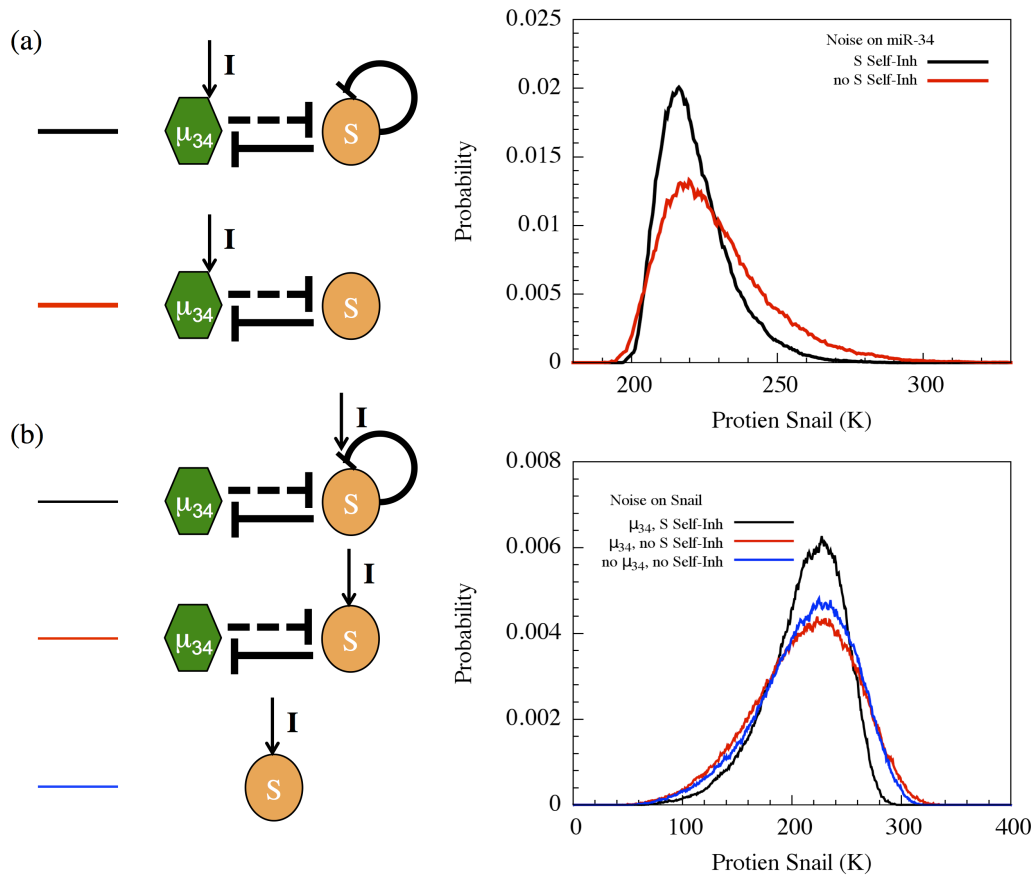
Fig SI8. miR-34/SNAIL module serves as a filter for external noise. The upper panel shows simulation results when the noisy signal is input to miR-34. The upper left diagram illustrates the two simulations, one with SNAIL self-inhibition and one without. The upper right diagram shows the distribution of the SNAIL levels. The lower panel shows simulations when the noisy signal is a direct input to SNAIL. The lower left diagram illustrates the three simulations: one with SNAIL self-inhibition, one without self-inhibition, and one without both miR-34 and SNAIL self-inhibition. The lower right diagram shows the distribution of the SNAIL levels in these three cases.

8. The role of auto-regulations

In this section, we studied the role of auto-regulation in the multi-stability of the circuits. More specifically, we removed the self-activation of ZEB, or the self-inhibition of SNAIL, and checked the resulting multi-stability of the miR-200/ZEB module, the miR-34/SNAIL module, and the combined circuit.

In the main article, we showed that the miR-34/SNAIL circuit is monostable. Here, without the self-inhibition of SNAIL, the circuit is still monostable (green shades in Table SI5, Fig SI8). It suggests that the self-inhibition of SNAIL does not alter the monostability of the circuit.

In main article, we showed that miR-200/ZEB circuit is tristable. But, without the self-activation of ZEB, the circuit can only be bistable (orange shades in Table SI5, Fig SI9a). We also tested the combined circuit without ZEB's self-activation, and found that it too can only be bistable (blue shades in Table SI5, Fig SI9b). If the self-activation of ZEB is kept with only one binding site, both the miR200-ZEB and the combined circuit are only bistable (purple shades in Table SI5, Fig SI9c, d). The results suggest that the cooperative self-activation of ZEB is essential for the tristability of miR-200/ZEB module and the combined circuit.

	Fig SI8, Fig SI9a	Fig SI9b	Fig SI9c, Fig SI9d
g_{m34} (K Molecules/Hour)	1.35	1.35	1.35
g_{mS} (Molecules/Hour)	25.0	90.0	90.0
S^0_{m34} (K Molecules)	300	300	300
S^0_{mS} (K Molecules)	---	200	200
g_{m200} (K Molecules/Hour)	2.5	2.1	2.1
g_{mZ} (Molecules/Hour)	90.0	62.5	12.5
Z^0_{m200} (K Molecules)	200	220	220
Z^0_{mZ} (K Molecules)	---	---	25

Table SI5. The parameters for the auto-regulation test. Only the adjusted parameters are listed here, and the rest parameters are listed in Table SI1 and Table SI4. Different colors highlight the parameters for different figures.
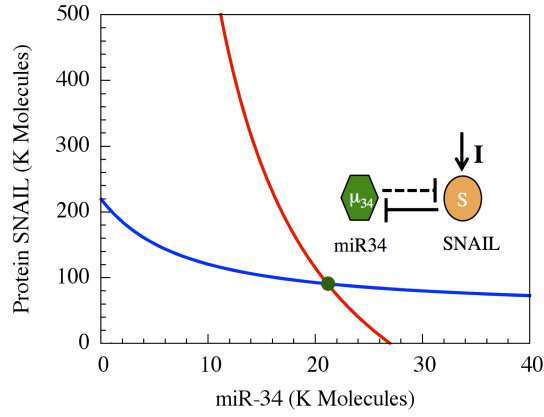
Fig SI9. Effects of the self-inhibition of SNAIL to the multistability of the circuit. Nullclines are plotted for the circuits without self-inihibition, otherwise similar to that in Fig SI7.
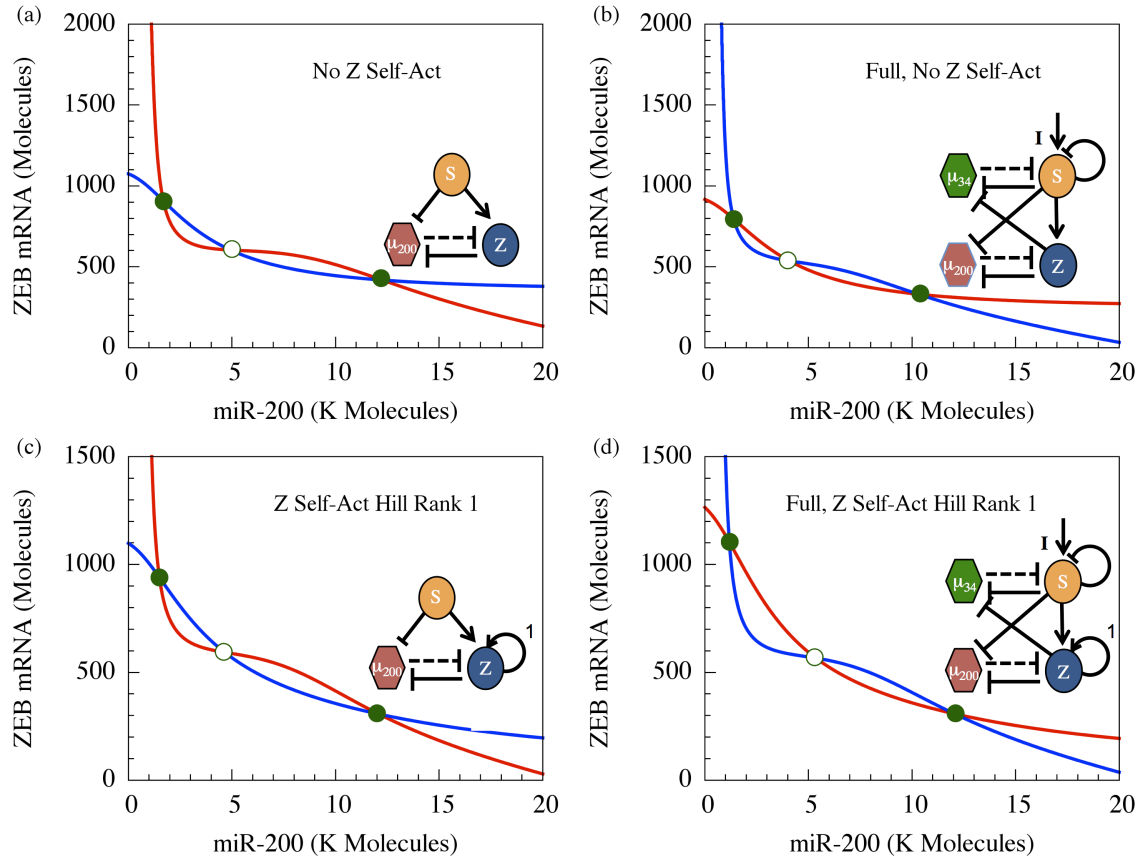

Fig SI10. Effects of the self-activation of ZEB on the multistability of the circuit. Nullclines are plotted for the circuit without self-activation (a, b), and with rank-one self-activation (c, d), otherwise similar to that in Fig SI7. Only the miR-200/ZEB circuit is analyzed in (a) and (c), and the combined circuit is analyzed in (b) and (d).

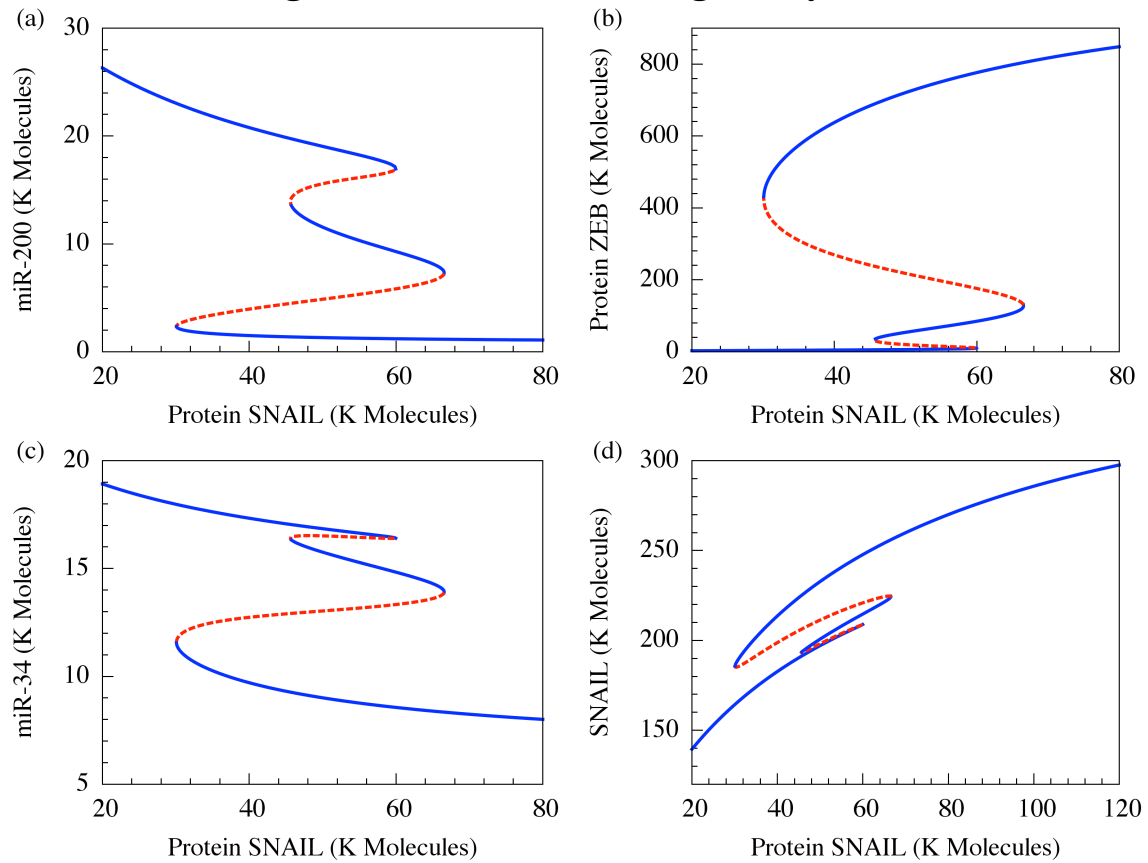# 9. Bifurcation diagrams of the combined regulatory unit

Fig SI11. Bifurcation plots for the levels of different molecules in the combined circuit driven by SNAIL. The plots are similar to Fig 4a, except that the y-axis is: (a) miR-200, (b) protein ZEB, (c) miR-34 and (d) protein SNAIL.

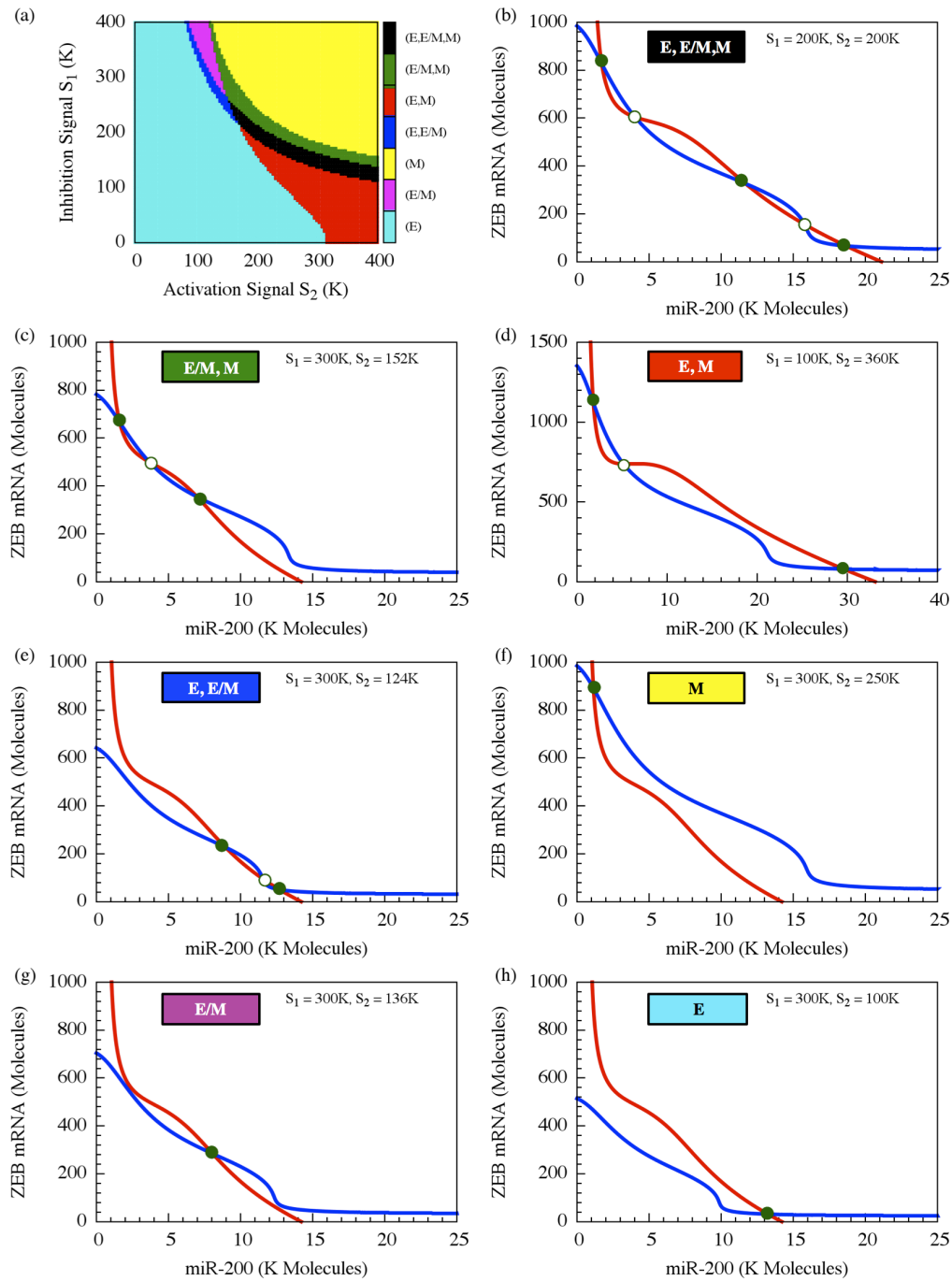# 10. Phase diagram of the mR-200/ZEB ternary switch

Fig SI12. Details of the different phases in the two-signal bifurcation plot for the miR-200/ZEB circuit. a) shows the two-signal bifurcation plot (also in Fig 4b in the main article). b) to h) show the nullclines for the circuit at different phases – one phase for tristability (b), three phases for bistability (c, d, e) and three phases for monostability (f,

g, h). For each graph, the input signals S_1 and S_2 were chosen in the corresponding phase. The nullclines are plotted in the same way as that in Fig SI7.

11. Coupling the miR-200/ZEB and the miR-34/SNAIL Modules

In the main article, we showed that the basic structure of the bifurcation plot for ZEB with respect to SNAIL is unaffected by including the transcriptional regulation of miR-34 by ZEB. This result arises because the dynamics of the miR-200/ZEB module solely depends on the SNAIL level. Second, the bifurcation plot for ZEB with respect to the external signal I, mainly shifts to the left for high levels of ZEB if ZEB inhibits miR-34 transcription; conversely, it is shifted to the right for high levels of ZEB if ZEB activates miR-34 transcription.

With the parameters from Table SI4, the transition from the "0" state (E or epithelial) to the "1" state (M or mesenchymal) goes through the intermediate state "1/2" (E/M). But on the other hand, we observed a direct reverse transition from the "1" state to the "0" state. So, the transitions between epithelial and mesenchymal states are not symmetric. It should be mentioned that the details of the transitions depend strongly on the parameters. Though we carefully chose parameters to match the values suggested by experiments, slightly different parameters choices can cause the transition dynamics to vary.

In a first example of this sensitivity, the ZEB threshold level for miR-200 transcriptional inhibition was changed from 220 K to 280 K molecules (Fig SI13a). Without the inhibition of ZEB acting on miR-34, the circuit does not have tristability at any signal level. But when the inhibition is included, the circuit can have tristability in some range of signal levels, and as before the transitions from the M to E do not go through the E/M state.

In the second example, the ZEB threshold level for miR-200 transcriptional inhibition is changed from 220 K to 180 K molecules (Fig SI13b). Without the inhibition of ZEB to miR-34, the circuit has tristability for a certain range of signal levels. Also, the transition from E to M goes through E/M, but the same is not true while going from M to E. With the inhibition of ZEB to miR-34 restored, the signal range for tristability becomes narrower, and the transitions from the E to M no longer go through the intermediate state (E/M) .

Although parameters play important roles in determining the dynamics, the inhibition of ZEB to miR-34 always makes it harder to transit back from the mesenchymal ("1") state at the same signal level. When the transition happens at a lower signal level, it is less likely to go through the intermediate state.
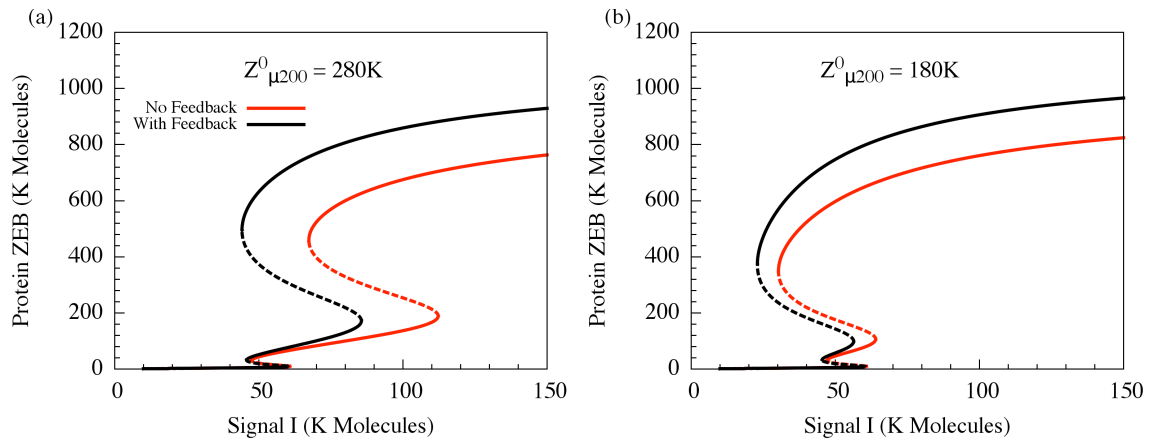

Fig SI13. The bifurcation plot of the combined circuit with different parameters. The figure is similar to Fig 5b in the main text. The simulations and parameters are also the same, except that the ZEB threshold for inhibiting miR-200 is changed to 280 K molecules for panel a, and 180 K molecules for panel b. The red lines show the bifurcation plot for the combined circuit, without any inhibition from ZEB to miR-34. The black lines show the bifurcation plot for the combined circuit after including the feedback inhibition of miR-34 by ZEB. It shows that different transition mechanisms can be observed in the same model upon varying the parameters.

Reference:

1. De Craene B & Berx G (2013) Regulatory networks defining EMT during cancer initiation and progression. *Nat Rev Cancer* 13(2):97-110.
2. Araki S, *et al*. (2010) TGF-beta1-induced expression of human Mdm2 correlates with late-stage metastatic breast cancer. *J Clin Invest* 120(1):290-302.
3. Eades G, *et al*. (2011) miR-200a regulates SIRT1 expression and epithelial to mesenchymal transition (EMT)-like transformation in mammary epithelial cells. *J Biol Chem* 286(29):25992-26002.
4. Elson-Schwab I, Lorentzen A, & Marshall CJ (2010) MicroRNA-200 family members differentially regulate morphological plasticity and mode of melanoma cell invasion. *PloS ONE* 5(10): e13176.
5. Kim D, *et al*. (2012) MicroRNA-34a Modulates Cytoskeletal Dynamics through Regulating RhoA/Rac1 Cross-talk in Chondroblasts. *J Biol Chem* 287(15):12501-12509.
6. Friedl P & Gilmour D (2009) Collective cell migration in morphogenesis, regeneration and cancer. *Nat Rev Mol Cell Biol* 10(7):445-457.
7. Friedl P & Wolf K (2010) Plasticity of cell migration: a multiscale tuning model. *J Cell Biol* 188(1):11-19.
8. Polytarchou C, Iliopoulos D, & Struhl K (2012) An integrated transcriptional regulatory circuit that reinforces the breast cancer stem cell state. *Proc Natl Acad Sci USA* 109(36):14470-14475.
9. Xu N, Papagiannakopoulos T, Pan GJ, Thomson JA, & Kosik KS (2009) MicroRNA-145 Regulates OCT4, SOX2, and KLF4 and Represses Pluripotency in Human Embryonic Stem Cells. *Cell* 137(4):647-658.
10. Chaffer CL, *et al*. (2013) Poised Chromatin at the ZEB1 Promoter Enables Breast Cancer Cell Plasticity and Enhances Tumorigenicity. *Cell* 154(1):61-74.
11. Wang GY, *et al*. (2013) Critical regulation of miR-200/ZEB2 pathway in Oct4/Sox2-induced mesenchymal-to-epithelial transition and induced pluripotent stem cell generation. *Proc Natl Acad Sci USA* 110(8):2858-2863.
12. Brabletz S, *et al*. (2011) The ZEB1/miR-200 feedback loop controls Notch signalling in cancer cells. *EMBO J* 30(4):770-782.
13. Vallejo DM, Caparros E, & Dominguez M (2011) Targeting Notch signalling by the conserved miR-8/200 microRNA family in development and cancer cells. *EMBO J* 30(4):756-769.
14. Bu P, *et al*. (2013) A microRNA miR-34a-regulated bimodal switch targets notch in colon cancer stem cells. *Cell Stem Cell* 12(5):602-615.
15. Lim SO, *et al*. (2011) Notch1 binds and induces degradation of Snail in hepatocellular carcinoma. *BMC Biol* 9:83.
16. Brabletz S & Brabletz T (2010) The ZEB/miR-200 feedback loop--a motor of cellular plasticity in development and cancer? *EMBO Rep* 11(9):670-677.
17. Siemens H, *et al*. (2011) miR-34 and SNAIL form a double-negative feedback loop to regulate epithelial-mesenchymal transitions. *Cell Cycle* 10(24):4256-4271.

18.	Bracken CP, *et al*. (2008) A double-negative feedback loop between ZEB1-SIP1 and the microRNA-200 family regulates epithelial-mesenchymal transition. *Cancer Res* 68(19):7846-7854.

19.	Burk U, *et al*. (2008) A reciprocal repression between ZEB1 and members of the miR-200 family promotes EMT and invasion in cancer cells. *EMBO Rep* 9(6):582-589.

20.	Hurteau GJ, Carlson JA, Roos E, & Brock GJ (2009) Stable expression of miR-200c alone is sufficient to regulate TCF8 (ZEB1) and restore E-cadherin expression. *Cell Cycle* 8(13):2064-2069.

21.	Peiro S, *et al*. (2006) Snail1 transcriptional repressor binds to its own promoter and controls its expression. *Nucleic Acids Res* 34(7):2077-2084.

22.	Guaita S, *et al*. (2002) Snail induction of epithelial to mesenchymal transition in tumor cells is accompanied by MUC1 repression and ZEB1 expression. *J Biol Chem* 277(42):39209-39216.

23.	Wels C, Joshi S, Koefinger P, Bergler H, & Schaider H (2011) Transcriptional Activation of ZEB1 by Slug Leads to Cooperative Regulation of the Epithelial-Mesenchymal Transition-Like Phenotype in Melanoma. *J Invest Dermatol* 131(9):1877-1885.

24.	de Herreros AG & Baulida J (2012) Cooperation, amplification, and feed-back in epithelial-mesenchymal transition. *BBA-Rev Cancer* 1825(2):223-228.

25.	Das S, Becker BN, Hoffmann FM, & Mertz JE (2009) Complete reversal of epithelial to mesenchymal transition requires inhibition of both ZEB expression and the Rho pathway. *BMC Cell Biol* 10.

26.	Aigner K, *et al*. (2007) The transcription factor ZEB1 (delta EF1) promotes tumour cell dedifferentiation by repressing master regulators of epithelial polarity. *Oncogene* 26(49):6979-6988.

27.	Gregory PA, *et al*. (2011) An autocrine TGF-beta/ZEB/miR-200 signaling network regulates establishment and maintenance of epithelial-mesenchymal transition. *Mol Biol Cell* 22(10):1686-1698.

28.	Taube JH, *et al*. (2010) Core epithelial-to-mesenchymal transition interactome gene-expression signature is associated with claudin-low and metaplastic breast cancer subtypes (vol 107, pg 15449, 2010). *Proc Natl Acad Sci USA* 107 (44): 19132-19132.

29.	Lu M, *et al*. (2013) Tristability in Cancer-Associated MicroRNA-TF Chimera Toggle Switch. *J Phys Chem B*.

30.	Levine E, Ben Jacob E, & Levine H (2007) Target-specific and global effectors in gene regulation by MicroRNA. *Biophys J* 93(11):L52-L54.

31.	Mitarai N, *et al*. (2009) Dynamic features of gene expression control by small regulatory RNAs. *Proc Natl Acad Sci USA* 106(26):10655-10659.

32.	Kim NH, *et al*. (2011) A p53/miRNA-34 axis regulates Snail1-dependent cancer cell epithelial-mesenchymal transition. *J Cell Biol* 195(3):417-433.

33.	Gregory PA, *et al*. (2011) An autocrine TGF-beta/ZEB/miR-200 signaling network regulates establishment and maintenance of epithelial-mesenchymal transition. *Mol Biol Cell* 22(10):1686-1698.

34.   Filipowicz W, Bhattacharyya SN, & Sonenberg N (2008) Mechanisms of post-transcriptional regulation by microRNAs: are the answers in sight? *Nat Rev Genet* 9(2):102-114.
35.   Duff C, Smith-Miles K, Lopes L, & Tian TH (2012) Mathematical modelling of stem cell differentiation: the PU.1-GATA-1 interaction. *J Math Biol* 64(3):449-468.
36.   Lipshtat A, Loinger A, Balaban NQ, & Biham O (2006) Genetic toggle switch without cooperative binding. *Phys Rev Lett* 96(18): 188101-4.
37.   Eden E, *et al*. (2011) Proteome half-life dynamics in living human cells. *Science* 331(6018):764-768.
38.   Yang E, *et al*. (2003) Decay rates of human mRNAs: correlation with functional characteristics and sequence attributes. *Genome Res* 13(8):1863-1872.
39.   Khanin R & Vinciotti V (2008) Computational modeling of post-transcriptional gene regulation by microRNAs. *J Comput Biol* 15(3):305-316.
40.   Gantier MP, *et al*. (2011) Analysis of microRNA turnover in mammalian cells following Dicer1 ablation. *Nucleic Acids Res* 39(13):5692-5703.
41.   Milo R, Jorgensen P, Moran U, Weber G, & Springer M (2010) BioNumbers-the database of key numbers in molecular and cell biology. *Nucleic Acids Res* 38: D750-D753.
42.   Schwanhausser B, *et al*. (2011) Global quantification of mammalian gene expression control. *Nature* 473(7347):337-342.
43.   Lim LP, *et al*. (2003) The microRNAs of Caenorhabditis elegans. *Genes Dev* 17(8):991-1008.
44.   Hill L, Browne G, & Tulchinsky E (2013) ZEB/miR-200 feedback loop: At the crossroads of signal transduction in cancer. *Int J Cancer* 132(4): 745-754.